Interim Report

Title: Investigations on the Effect of Steady and Pulsed Surface Thermal Perturbations on the Hypersonic Flow-Field over a Flat Plate and a Sharp Cone

AFOSR/AOARD Reference Number: AOARD- FA4869-08-1-4032

AFOSR/AOARD Program Manager: Dr. Ponnappan

Period of Performance: 2008 - 2009

Submission Date: 10th March 2010

Principal Investigator: Prof. G. Jagadeesh
Dept. of Aerospace Engineering
Indian Institute of Science, Bangalore – 560 012, INDIA

Report Documentation Page

Form Approved
OMB No. 0704-0188

1. REPORT DATE	2. REPORT TYPE	3. DATES COVERED
29 MAR 2010	**Final**	**12-02-2008 to 10-03-2010**

4. TITLE AND SUBTITLE
Shock tunnel investigations on the effects of thermal bumps in the flow field around a flat plate

5a. CONTRACT NUMBER
FA48690814032

5b. GRANT NUMBER

5c. PROGRAM ELEMENT NUMBER

6. AUTHOR(S)
Gopalan Jagadeesh

5d. PROJECT NUMBER

5e. TASK NUMBER

5f. WORK UNIT NUMBER

7. PERFORMING ORGANIZATION NAME(S) AND ADDRESS(ES)
Indian Institute of Science,Bangalore, Karnataka State,Bangalore,India,IN,560 012

8. PERFORMING ORGANIZATION REPORT NUMBER
N/A

9. SPONSORING/MONITORING AGENCY NAME(S) AND ADDRESS(ES)
Asian Office of Aerospace Research & Development, (AOARD), Unit 45002, APO, AP, 96338-5002

10. SPONSOR/MONITOR'S ACRONYM(S)
AOARD

11. SPONSOR/MONITOR'S REPORT NUMBER(S)
AOARD-084032

12. DISTRIBUTION/AVAILABILITY STATEMENT
Approved for public release; distribution unlimited

13. SUPPLEMENTARY NOTES

14. ABSTRACT
The effects of both steady and pulsating thermal bump presence in the vicinity of the boundary layer of generic bodies have been investigated. The variation of surface static pressure along a sharp leading edge flat plate at angle of attack (10 deg.) has been measured in the presence of both steady and pulsating thermal bump. In these studies, both argon and air have been used as test gases. A heating element capable of reaching 1280 K in an area of 13 mm2 is used to generate a steady thermal bump within the boundary layer of the flat plate model. A dielectric barrier discharge (DBD) over an area of 10 sq mm is used for generating pulsating thermal bump (~ 10 W/sqcm at 6, 8 and 19 kHz) near the leading edge of the flat plate. The static pressure distribution along the flat plate is measured at different pulsing frequency of DBD at hypersonic Mach numbers. The pressure field in the presence of steady thermal bump appears to be oscillatory. At some locations downstream of the bump the static pressure decreased by ~ 25 -30% while it increased by 10-15% at other locations in the vicinity of the hot spot. However substantial reductions in the downstream pressure (30 -50%) have been measured on the flat plate in the presence of oscillating thermal bump. The reduction appears to be strongly dependent on the pulsing frequency. The pressure reduction seems to be better with argon as test gas compared to the experiments with dry air. Due to the effects of electromagnetic interference and inherently lower values surface convective heat transfer rates on the flat plate in the presence of oscillatory thermal bump could not be measured. However, surface heat transfer rates on a cone-cylinder model in the presence of a steady thermal bump (40 W/sq cm) near the apex of the sharp cone has been measured.

15. SUBJECT TERMS **Hypersonics, Shock Tunnels, Thermal bump**					
16. SECURITY CLASSIFICATION OF:			17. LIMITATION OF ABSTRACT	18. NUMBER OF PAGES	19a. NAME OF RESPONSIBLE PERSON
a. REPORT **unclassified**	b. ABSTRACT **unclassified**	c. THIS PAGE **unclassified**	**Same as Report (SAR)**	**30**	

Standard Form 298 (Rev. 8-98)
Prescribed by ANSI Std Z39-18

Abstract

The effect of both steady and pulsating thermal bump presence in the vicinity of the boundary layer of generic bodies have been investigated in the IISc hypersonic shock tunnel. The variation of surface static pressure along a sharp leading edge flat plate at angle of attack (10 deg.) has been measured in the presence of both steady and pulsating thermal bump. In these studies both argon and air have been used as test gases. A heating element capable of reaching 1280 K in an area of 13 mm^2 is used to generate a steady thermal bump within the boundary layer of the flat plate model. A dielectric barrier discharge (DBD) over an area of 10 mm^2 is used for generating pulsating thermal bump (~ 10 W/cm^2 at 6, 8 and 19 kHz) near the leading edge of the flat plate. The static pressure distribution along the flat plate is measured at different pulsing frequency of DBD at hypersonic Mach numbers. The pressure field in the presence of steady thermal bump appears to be oscillatory. At some locations downstream of the bump the static pressure decreased by ~ 25 -30% while it increased by 10-15% at other locations in the vicinity of the hot spot. However substantial reductions in the downstream pressure (30 -50%) have been measured on the flat plate in the presence of oscillating thermal bump. The reduction appears to be strongly dependent on the pulsing frequency. The pressure reduction seems to be better with argon as test gas compared to the experiments with dry air. Due to the effects of electromagnetic interference and inherently lower values surface convective heat transfer rates on the flat plate in the presence of oscillatory thermal bump could not be measured. However, surface heat transfer rates on a cone-cylinder model in the presence of a steady thermal bump (40 W/cm^2) near the apex of the sharp cone has been measured. Drastic reduction (60%) near the cone cylinder junction has been measured in the presence of the hot spot near the cone apex at Mach 6. Evaluating the precise reasons for the observed variation in the measured values of static pressure and convective heating rates, more experiments and wavelet based data analysis to find out the additional frequencies in the hypersonic flow field introduced because of thermal bump are some of the aspects that will be addressed in future studies.

Introduction

The main goal of the present project is to systematically investigate the effect of a localized hot spot (both steady and pulsating) on the hypersonic flow field. This steady or pulsating hot spot is referred as thermal bump. In the initial results that were presented in the previous year (2008-09) we have used a heating element and a localized electric discharge to generate the thermal bump on a sharp leading edge flat plate at zero degree angle of incidence. The measurements that were carried out in the IISc hypersonic shock tunnel indicated some trends but largely the data was influenced by electromagnetic interference especially the experiments wherein electric discharge was used to generate thermal bumps. Moreover the surface pressure and the heat transfer rate values at the reported freestream conditions were very low at zero angle of incidence, such that the data was highly uncertain even without thermal bump. With the present set of experiments the previous issues with the measurements have been addressed systematically. Sensible measurements of surface pressures over a flat plate at an angle of 10^0 with the freestream have been done with and without thermal bump near the leading edge. The steady thermal bump is created by means of a heating element and the pulsed thermal bump is created by means of dielectric barrier discharge (plasma) between electrodes with high potential difference maintained between them by a high voltage device. Surface heat transfer rates have been measured on a sharp cone model with and without thermal bump. While the heating element does not involve high voltage devices, for experiments with the dielectric barrier discharge the electromagnetic interference was brought down by proper shielding of cables and by ensuring high values of measured quantities. The details of the experiments and discussions on the results with and without thermal bump will be presented subsequently.

Objectives:

The main aim of the present work is to understand the basic streamwise vortex generation and the viscous interactions associated with the presence of a thermal bump in a hypersonic boundary layer. The specific aims of the study are:

1. Understanding the basic gasdynamic implications of having a thermal bump (both surface heating and volumetric heating) in the flow field around a sharp leading edge flat plate at hypersonic Mach number (Mach 6 & 8), by carrying out comprehensive experiments in the IISc hypersonic shock tunnel using both argon and air as test gases.
2. Design and development of electrical and plasma energy sources for creating both 2-D and 3-D thermal bumps over the flat plate model during shock tunnel testing.
3. Measure the surface convective heat transfer rates and surface static pressures in the presence of both steady state and oscillating thermal bumps at hypersonic speeds using generic models like flat plate or sharp cone/cylinder.

Experimental Methodology:

Experiments on the flat plate model are done in IISc shock tunnel HST-5. This is a conventional shock tunnel which operates with the help of a metal diaphragm separating the driver and driven sections of a shock tube. The HST5 shock tunnel consists of a driver section, a driven section, a conical nozzle and a test section (includes the dump tank). The driver and driven sections are of 3 m and 6.19 m long while the inner diameter and wall thickness of the shock tube are

103 mm and 12 mm respectively. The conical nozzle consists of converging and diverging portions with area ratio corresponding to a Mach 6 nozzle. The converging and diverging portions are respectively 50 mm and 720 mm long. Aluminium diaphragms of 1 mm and 3 mm thickness with a depth of preferential fracture groove equal to 1/3rd of the thickness in the shape of a plus sign separates the driver and driven sections. The groove facilitates nice petal formation in the ruptured diaphragm and provides good repeatability of test conditions. The fill pressure is 2.5 bar and 7.5 bar (gauge) for 1 mm and 3 mm diaphragms respectively. The driven section is filled with test gas (air) at 200 mm of Hg. The entire tunnel portion of HST5 including nozzle test section dump tank is maintained at pressure below 10^{-5} mbar before the start of a run. Figures 1&2 show photographs of the nozzle-dump-tank assembly and the panoramic view of the HST5 hypersonic shock tunnel used in the present studies.

Fig.1: Photograph showing the tunnel portion of the HST5 shock tunnel.

Fig.2: The panoramic view of hypersonic shock tunnel HST5.

With the PCB pressure transducers used, pressures of the order of 1000 Pa can be measured with good accuracy. Thus it was decided to restrict to a Mach 6.2 nozzle (for air as test gas), with a freestream stagnation pressure of around 29 bar for which the freestream pressure would be around 1400 Pa. With the flat plate being placed at an angle of 10^0 to the

freestream, the measured surface pressure would be more than 3000 Pa, for which the sensors respond with good accuracy. The required freestream conditions were achieved by setting proper driver and driven pressures. A calibration of the tunnel was done for the decided freestream conditions with a pitot rake measurement. A rake of 12 pitot probes spanning the diameter of the nozzle (300 mm) was placed facing the freestream. The pitot pressures were measured by means of kulite transducers which are less noisy. Apart from this, the shock tube pressures were measured at 2 locations, one near the end of the driven section and another one, a little ahead in the shock tube (separated by 205 mm), so as to measure the flow stagnation pressure as well as the shock speed inside the shock tube. The repeatability of the experiments is ensured by monitoring the diaphragm rupture pressures. Air and Argon have been used as test gas in the present study. Figures 3 and 4 show the typical stagnation pressures measured in the test section and at the end of the shock tube respectively.

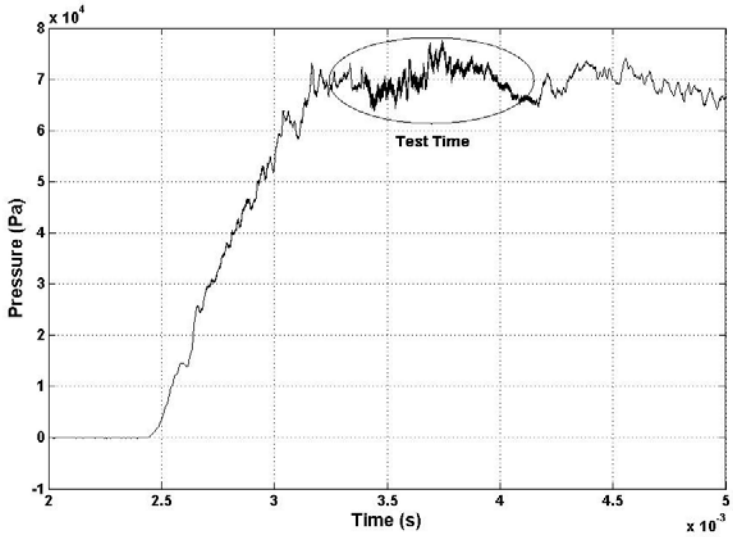

Figure.3: Typical pitot signal measured in the shock tunnel test section

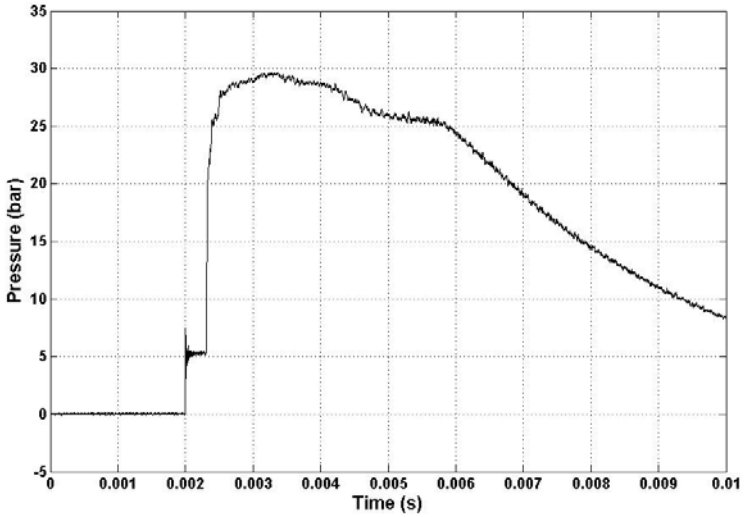

Figure.4: Typical reservoir pressure or freestream stagnation pressure (p_5) signal

The freestream conditions are estimated by means of isentropic and normal shock relations from the measured reservoir pressure p_5 (stagnation pressure in the shock tube before expanding through nozzle, also referred as P_0), pitot pressure (pressure behind normal shock) and shock Mach number in the shock tube. The freestream conditions thus estimated are tabulated in the following tables for experiments with the flat plate model, with Table.1 for the experiments with air as test gas, Table.2 with argon.

Note: The repeatability of the pitot and the shock tube pressure measurements are affected by the driver and driven pressures. While the driven pressure is fixed, the driver pressure is the rupture pressure of the diaphragm separating the sections of the shock tube. It was ensured that the rupture pressure does not vary much between the runs. The rupture pressure was observed to be around 34 bar for most of the runs, while it was 33 bar or 35 bar for a few runs. From the pitot rake and shock tube measurements, the freestream conditions for each of the observed rupture pressure are estimated. It was observed that of the 12 sensors in the pitot rake, 8 sensors were in the core and measured pressures with a maximum variation of ±5.6% between them. The outer 4 sensors had a variation of more than 10% from the others. The core region was thus estimated to have a diameter of 175 mm. Due to this spatial constraint it was not possible to have a pitot measurement along with the model during the experiments with flat plate. Thus the freestream conditions for the experiments are reported based on the observed diaphragm rupture pressure.

Table. 1: Freestream conditions with air as test gas

Run no	**M_∞**	**P_0 (bar)**	**T_0 (K)**	**P_∞ (Pa)**	**T_∞ (K)**	**ρ_∞ (kg/m3)**	**Re_∞x106 /m**
02	6.25	29.1	1474.2	1450.8	167.3	0.0302	4.30
06	6.26	29.39	1483.3	1451	167.8	0.0301	4.28
07	6.25	29.1	1474.2	1450.8	167.3	0.0302	4.30
09	6.25	29.1	1474.2	1450.8	167.3	0.0302	4.30
12	6.26	29.39	1483.3	1451	167.8	0.0301	4.28
13	6.25	29.1	1474.2	1450.8	167.3	0.0302	4.30
35	6.25	29.1	1474.2	1450.8	167.3	0.0302	4.30
36	6.26	29.39	1483.3	1451	167.8	0.0301	4.28
44	6.26	29.39	1483.3	1451	167.8	0.0301	4.28
45	6.26	29.39	1483.3	1451	167.8	0.0301	4.28
49	6.26	29.39	1483.3	1451	167.8	0.0301	4.28

Note:

Runs 02, 06 are experiments without plasma.

Runs 07 and 09 are experiments with plasma at 8000 Hz

Runs 12 and 13 are experiments with plasma at 19000 Hz

Runs 35 and 36 are experiments with plasma at 6000 Hz, with actuator of 0.5 cm.

Runs 44, 45 and 49 are experiments with glow plug mode; Runs 44 and 45 are with glow plug on and Run 49 is with glow plug off.

Table. 2: Freestream conditions with argon as test gas

Run no	**M_∞**	**P_0 (bar)**	**T_0 (K)**	**P_∞ (Pa)**	**T_∞ (K)**	**ρ_∞ (kg/m3)**	**Re_∞x106 /m**
04	9.02	25.93	2208.5	633.9	78.13	0.0390	9.90
05	9.07	26.26	2228.4	625.7	78.03	0.0386	9.86
10	9.02	25.93	2208.5	633.9	78.13	0.0390	9.90
11	9.02	25.93	2208.5	633.9	78.13	0.0390	9.90
14	9.07	26.26	2228.4	625.7	78.03	0.0386	9.86
40	9.07	26.59	2248.6	633.6	78.74	0.0387	9.83
41	9.07	26.59	2248.6	633.6	78.74	0.0387	9.83
46	9.07	26.59	2248.6	633.6	78.74	0.0387	9.83
47	9.07	26.59	2248.6	633.6	78.74	0.0387	9.83
48	9.07	26.59	2248.6	633.6	78.74	0.0387	9.83

Note:

Runs 04, 05 are experiments without plasma.

Runs 10 and 11 are experiments with plasma at 8000 Hz

Run 14 is experiment with plasma at 19000 Hz

Runs 40 and 41 are experiments with plasma at 6000 Hz, with actuator of 0.5 cm.

Runs 46, 47 and 48 are experiments with glow plug mode; Runs 46 and 47 are with glow plug on and Run 48 is with glow plug off.

Experiments with flat plate:

Test model:

The test model has a flat surface of length 20 cm and spans 12 cm, and is exposed to the freestream at 10^0. The model is of 5 cm thickness to accommodate the sensors. It is made of insulating material (Hylem). Figure.5 shows the schematic of the model with the locations of the sensors and the thermal bump (not to scale). The model is equipped with 2 rows of

PCB pressure sensors, one along the centre line, and the other along a line, 3 cm span wise from the centre line as shown in Figure.5. The centre row of pressure sensors is labeled as Array A, and the side on as Array B. Each row has 5 sensors, each spaced 2 cm from each other, with the first sensor at a distance of 9 cm from leading edge. The model is also equipped with 2 rows of platinum thin film sensors painted on a Macor substrate. The measured heat transfer rate values were very low for the selected enthalpy and the angle of attack of the flat plate, and were subject to electromagnetic interference with plasma despite shielding the cables. The data is thus less reliable and is not reported. Figure.6 shows the photograph of the model (top view).

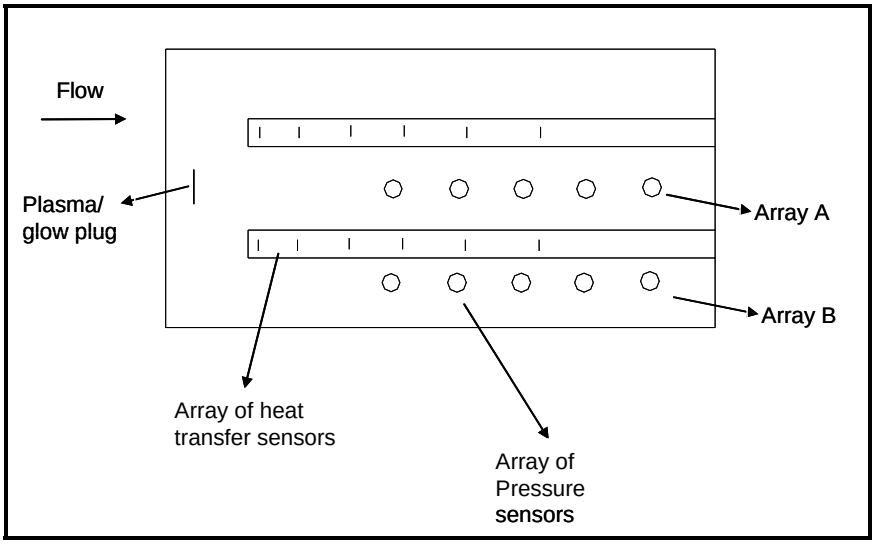

Figure.5: Schematic of the flat plate model (not to scale)

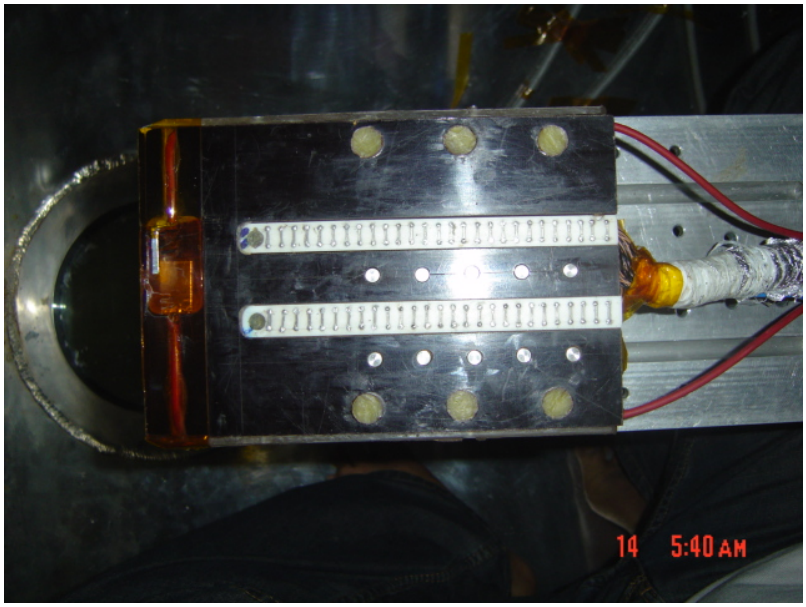

Figure.6: Photograph of the model mounted in the tunnel (top view)

Generating pulsating thermal bump:

Investigations are done with both steady as well as pulsed thermal perturbation. The pulsed thermal bump is created by means of pulsed plasma, generated by dielectric barrier discharge (DBD), at a distance of 5 mm from the leading edge (at span wise centre). DBD is the electric discharge between two electrodes separated by an insulating dielectric barrier. It needs a high voltage alternating current source (the source used can give up to 25 kV peak, 50 mA). Figure.7 shows the block diagram of the pulsed plasma generation and control unit. The plasma is controlled from a PC through a National Instruments Data Acquisition system interface. While DBD can be made in any configuration, for the present experiments a typical planar configuration wherein two parallel plates of electrodes are placed on the surface with a dielectric barrier (kapton tapes) between them. The electrodes and the dielectric layers are so thin that the entire setup is almost level with the surface as can be seen in Figure.8, which shows the plasma generated on the model surface near the leading edge. The effect of plasma actuator length is investigated by having actuators of lengths 15 mm and 5 mm. The effect of pulsing frequency is also investigated.

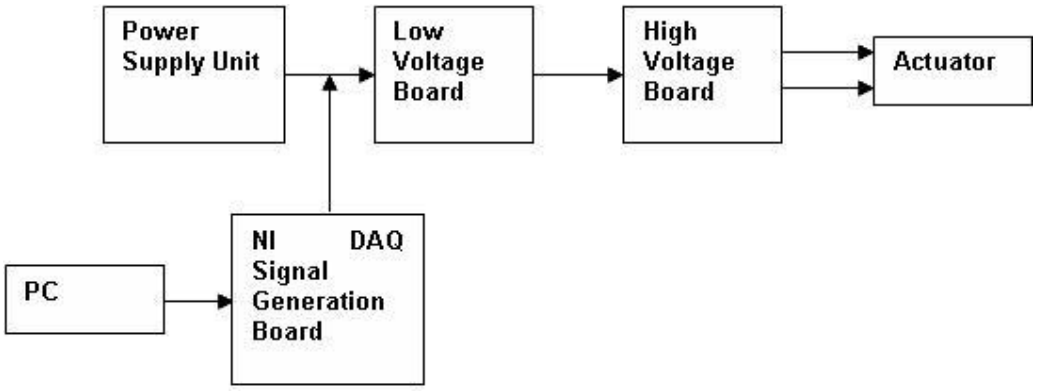

Figure.7: Block diagram of the pulsed plasma generation and control unit

Figure.8: Photograph of the plasma on the model surface near the leading edge

The steady thermal bump is created by means of a heating element (commercially available glow plug). The heating element is placed in a way such as to have a point of high temperature near the leading edge (approximately 5 mm) at the span wise centre. Figure.9 shows the way by which the heating element is accommodate in the model. For the heating element to be placed as a point source of high temperature it was required t keep it vertical with a support. A hole had to be drilled in the model to accommodate the heating element, which is placed in flush with the surface. A small clearance is given in the hole so as not to keep the hylem (material of the model) in direct contact with the heating element at high temperatures.

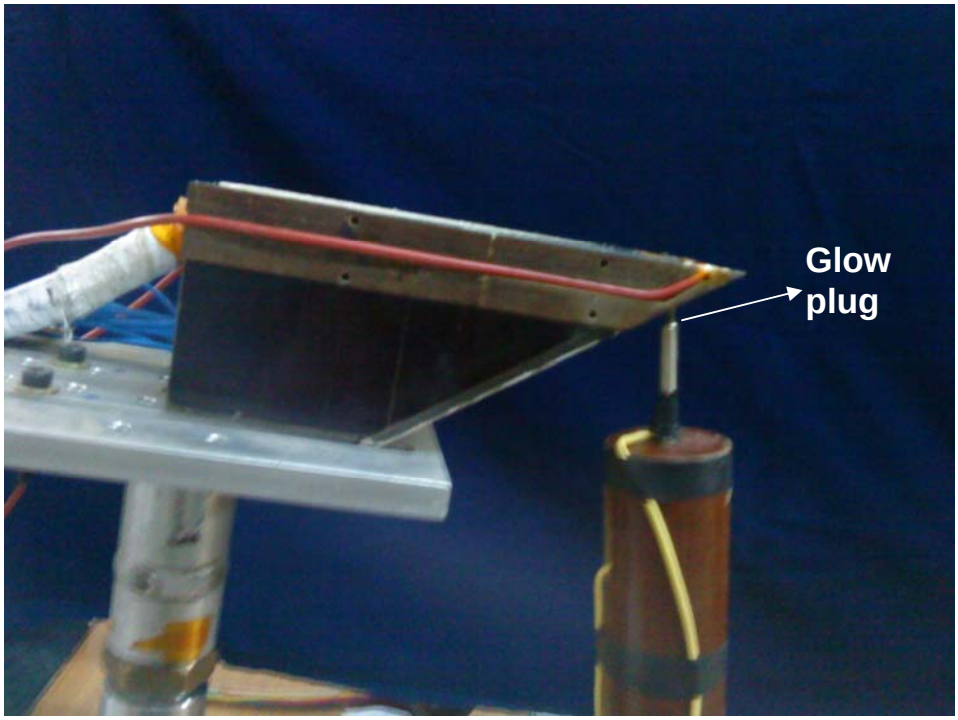

Figure.9: Photograph of the model with the mounting arrangement for the steady thermal bump (heating element)

Surface pressure measurements:

The surface pressures over the flat plate are measured using PCB pressure sensors. Measurements are made for the base case without thermal bump and for the case with thermal bump. For the case of the experiments with steady thermal bump, the model had a hole near the leading edge to accommodate the heating element (as discussed before). Thus to account for the cavity effect, these experiments are reported separately along with separate measurements for the base case too and are not compared with the measurements with the model for pulsed plasma (with and without plasma). 2 to 3 experiments are done per each case to ensure repeatability. Figure.10 shows the typical repeatable signals for a sensor for 2 runs without plasma, with air as test gas. Figure.11 shows the base case pressure without plasma along the length of the flat plate on both the arrays A and B, Figure.9a with air as test gas and 9b with argon as test gas.

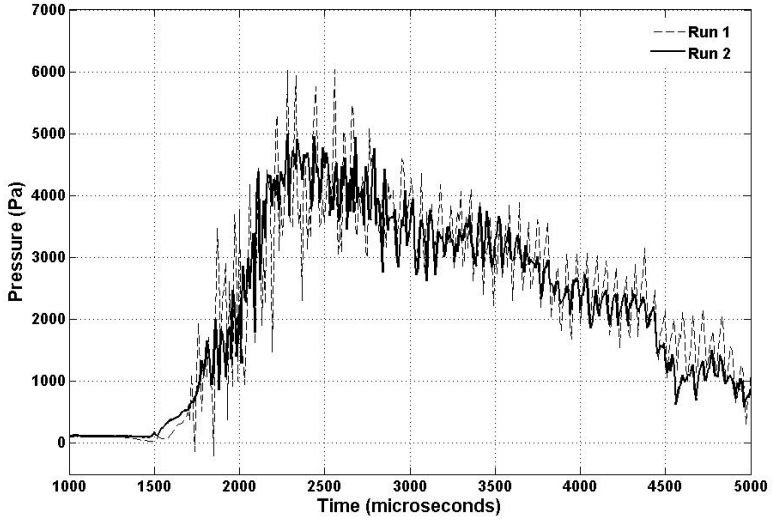

Figure.10: Repeatability of pressure signals in sensor 3 in the centre array without plasma, with air as test gas.

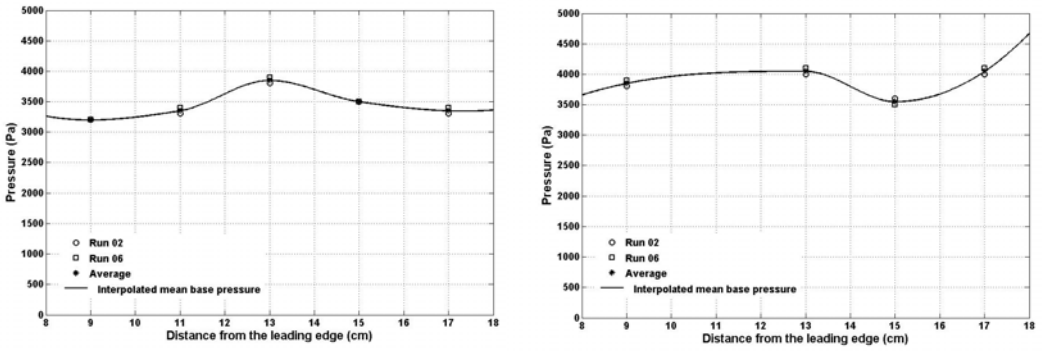

(a) Array A Array B

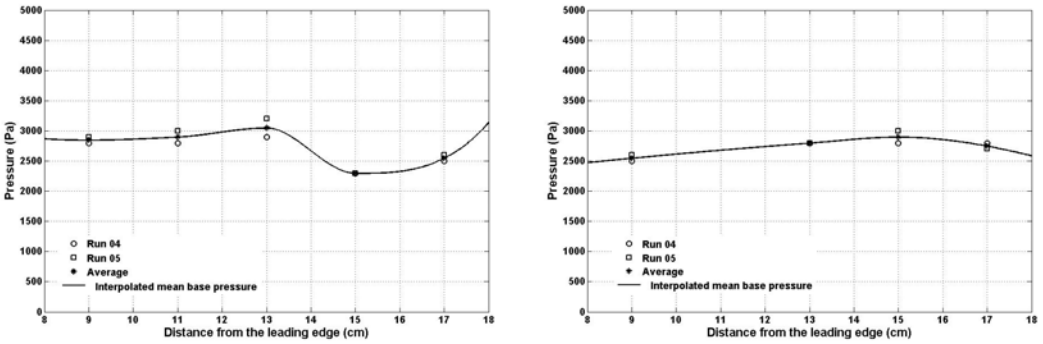

(b) Array A Array B

Figure.11: Pressure measurements along the length of the flat plate without thermal bump (plasma model); (a) Test gas- Air, (b) Test gas- Argon

It is observed from these base pressure measurements that there is a considerable difference in pressures between the two arrays of sensors (for same distances from the leading edge), which is a possible indicator of 3-D flow field. Further, even within the same array, there are considerable differences in the base pressure values. This is one issue that has to be addressed in the near future.

The location of the plasma was close to the leading edge (5 mm) and was located at the span wise centre. 2 different lengths of the plasma actuator are experimented, one with 15 mm and other with 5 mm. Also the effect of pulsing frequency was investigated by operating the 15 mm actuator at 2 different frequencies, 8 kHz and 19 kHz. The 5 mm actuator was operated at 6 kHz, which was the resonant frequency of the device. Figure.12 shows a comparison of the signals measured by the 3rd sensor in Array A, with and without plasma, for actuator length of 15 mm with air as test gas.

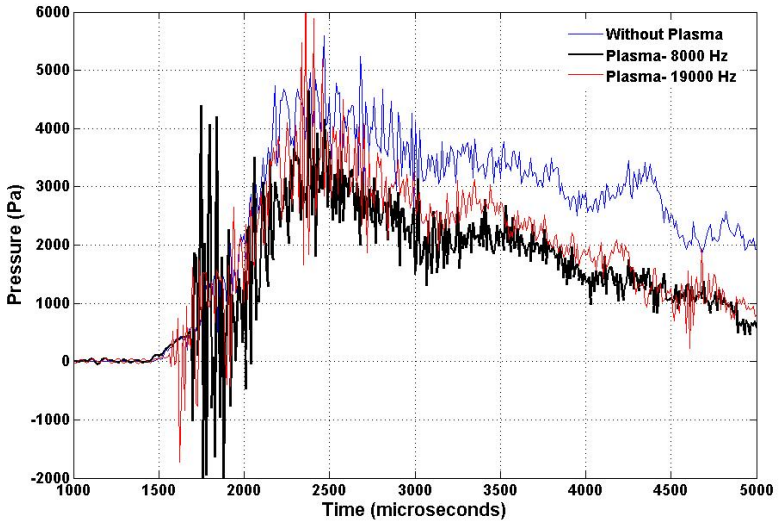

Figure.12: Pressure signals measured by sensor 3 in the centre array with and without plasma, with actuator of 15 mm length, with air as test gas

Clearly the pressure signals are not affected by electromagnetic interference. It can also be seen that there has been a considerable change in the measured signal by the presence of plasma, and also that the plasma pulsing frequency has a role to play. The effect of plasma frequency (with 15 mm actuator) can be seen in Figure.13 with air as test gas and in Figure.14 with argon as test gas. The effect of the length of the actuator is investigated by comparing the pressures for the cases with actuators of length 5 mm and 15 mm, each of which is operated at their resonant frequencies. Figure.15 shows the comparison for the case with air as test gas, and Figure.16with argon. The results of experiments with steady thermal bump (glow plug) are summarized in Figures 17 and 18. ***Note*:** The surface pressures are normalized by freestream pressures of the corresponding run and the distances are normalized by span length.

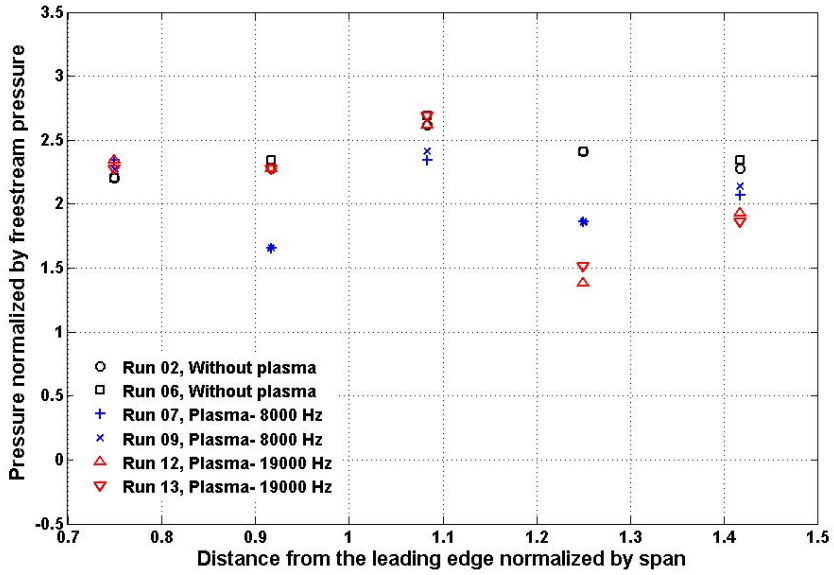

Array A

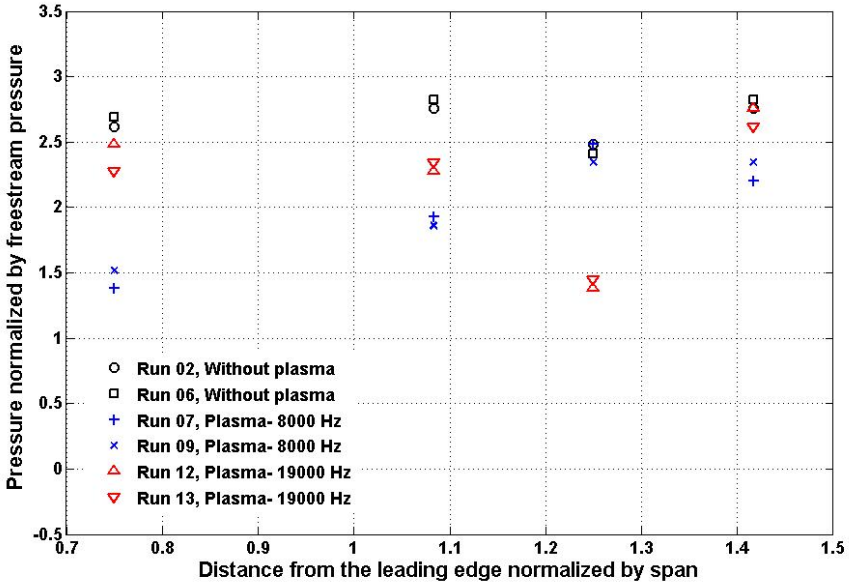

Array B

Figure.13: Effect of plasma pulsing frequency with air as test gas (15 mm actuator)

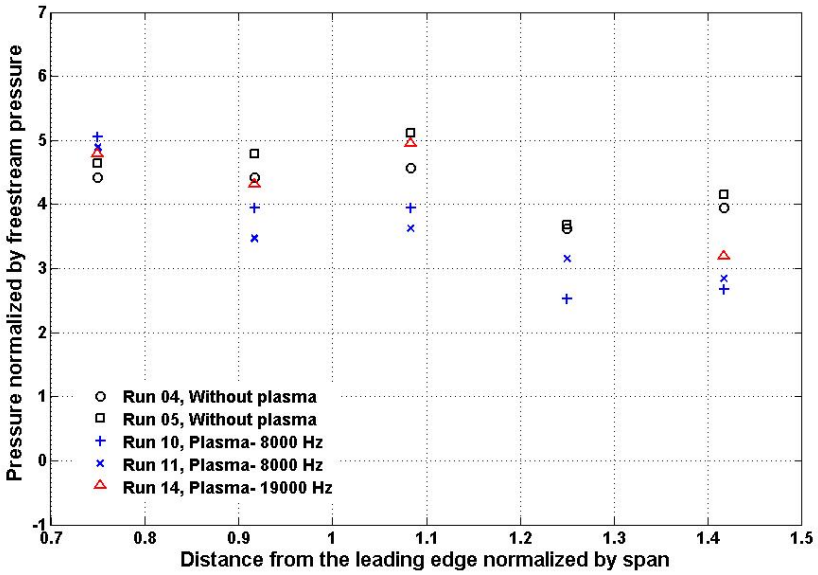

Array A

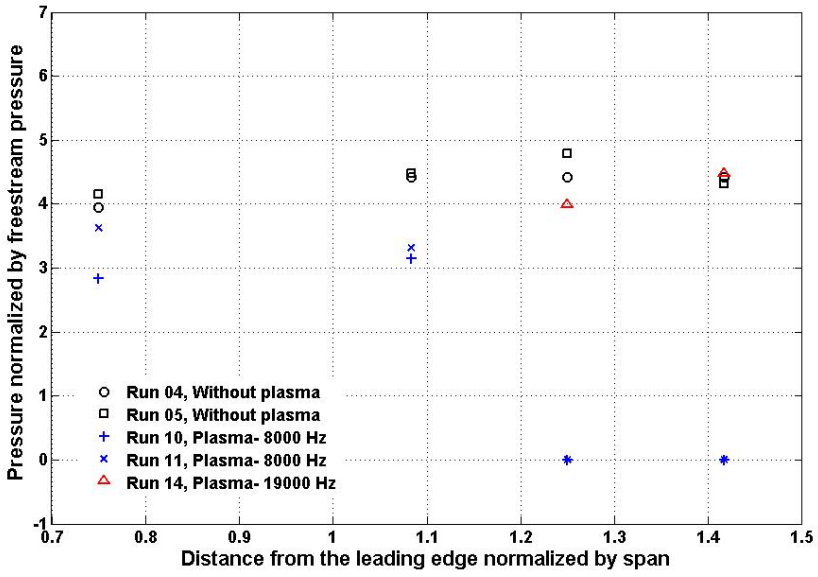

Array B

Figure.14: Effect of plasma pulsing frequency with argon as test gas (15 mm actuator)

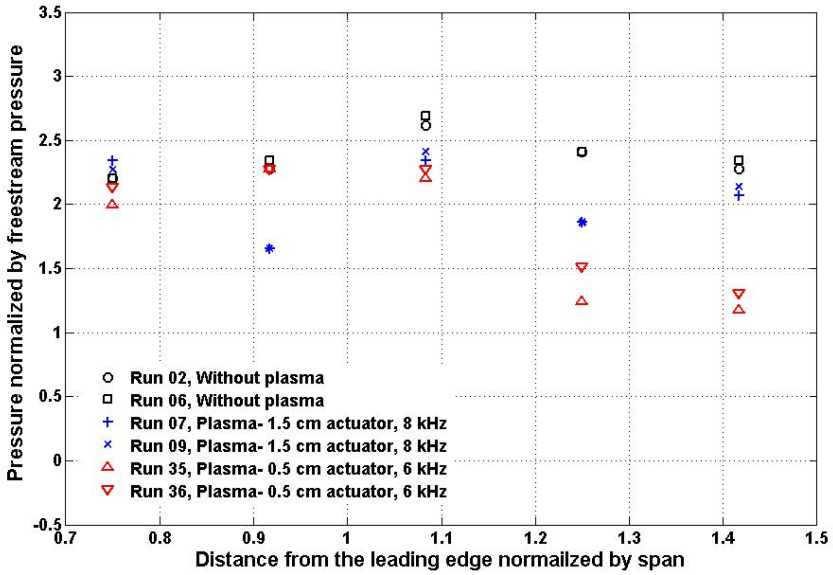

Array A

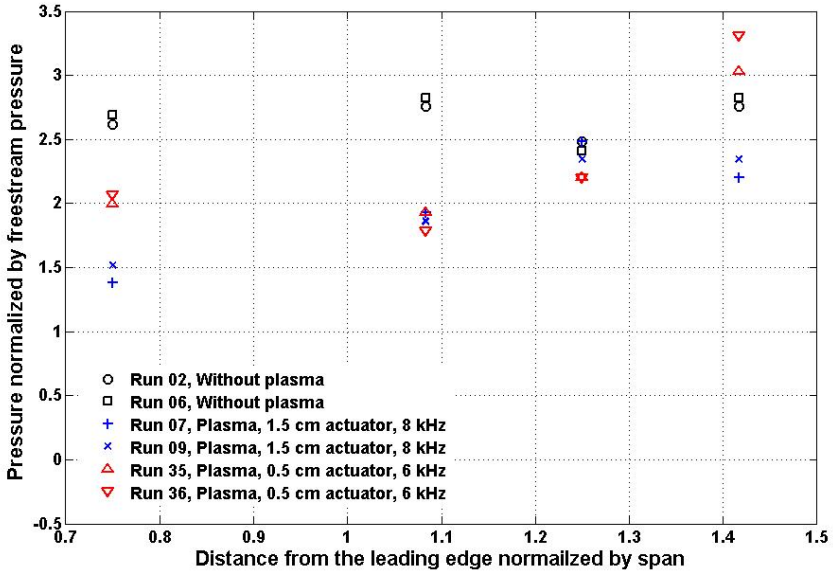

Array B

Figure.15: Effect of actuator length with air as test gas

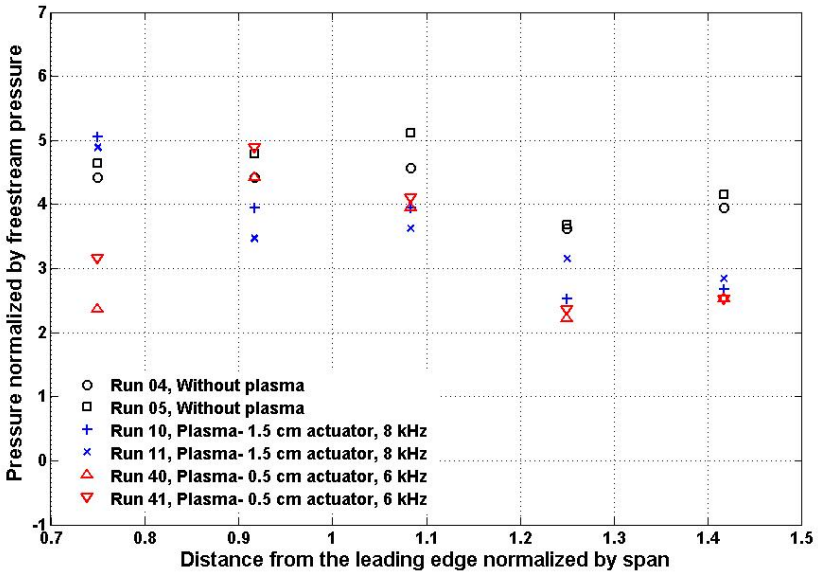

Array A

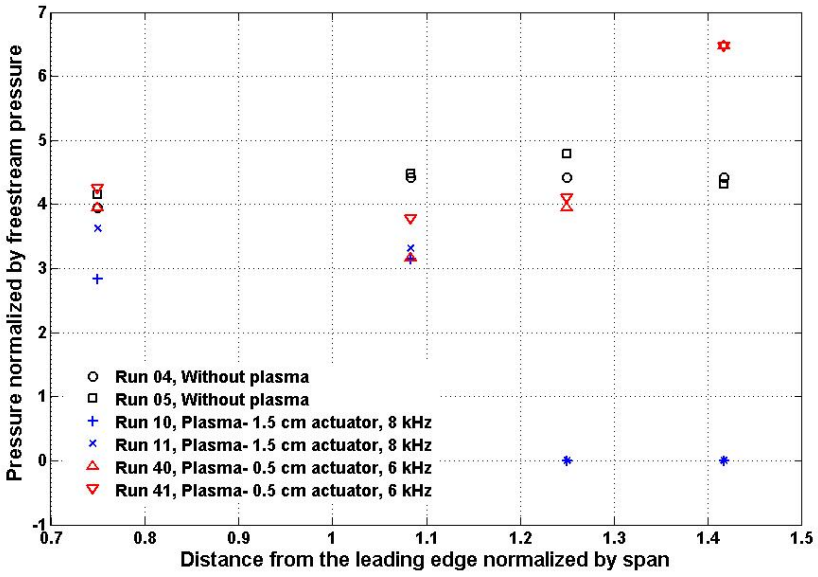

Array B

Figure.16: Effect of actuator length with argon as test gas

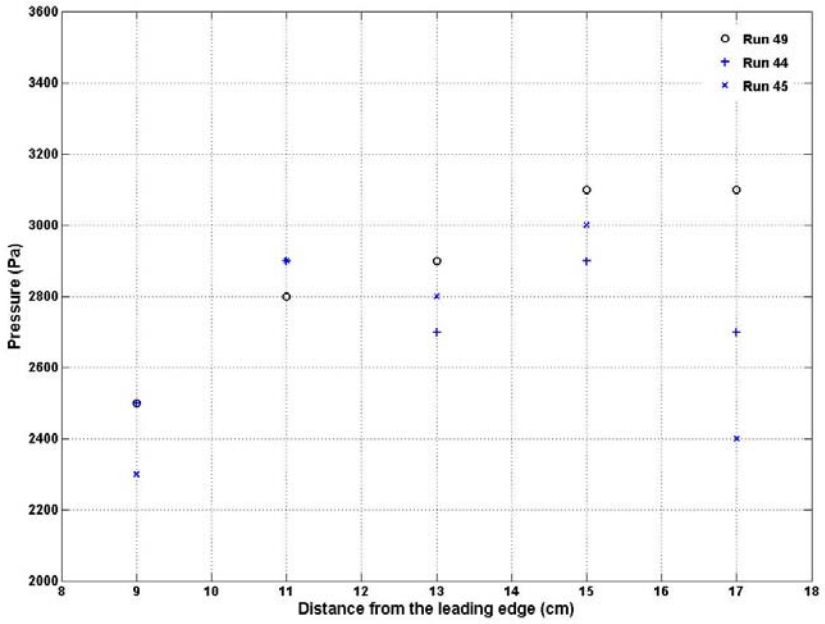

Array A

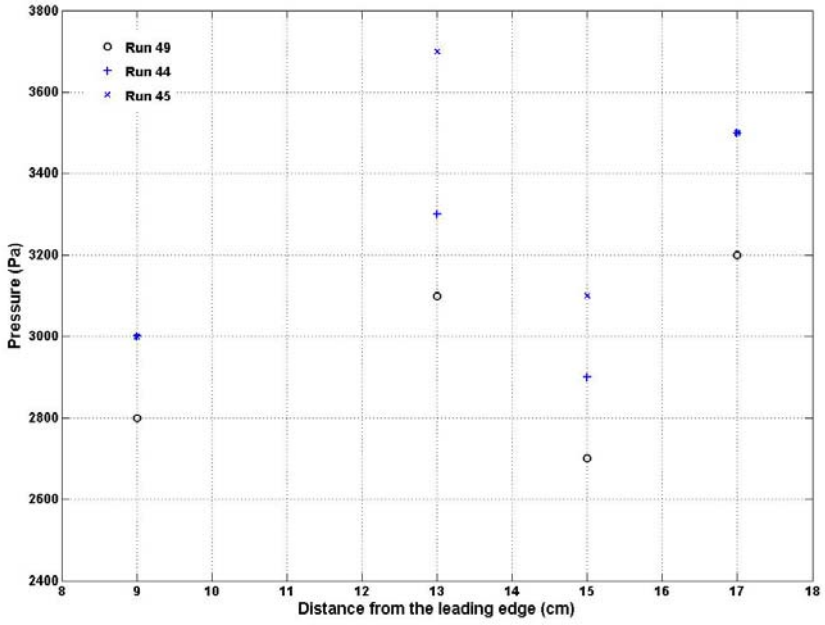

Array B

Figure.17: Effect of steady thermal bump (glow plug) with air as test gas; Run49- without thermal bump, Run 44 and 45- with thermal bump

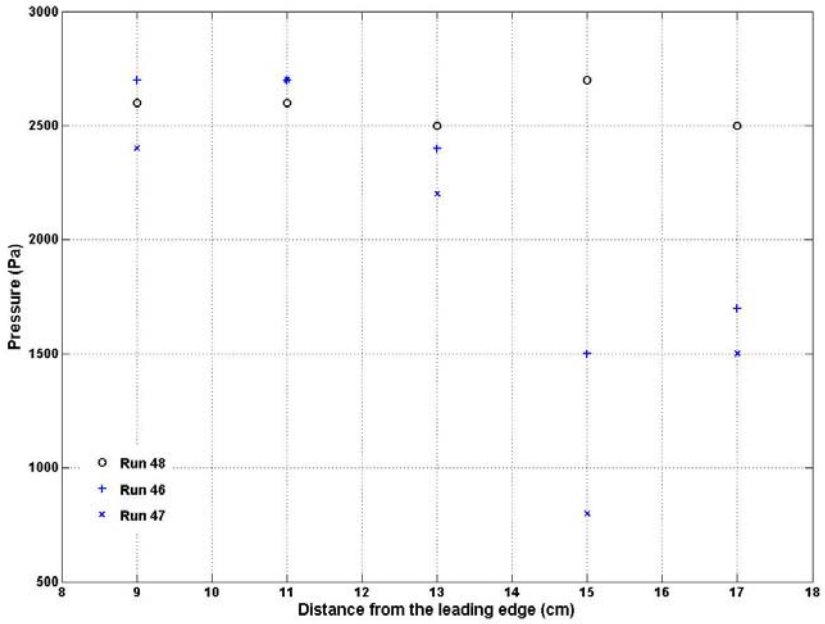

Array A

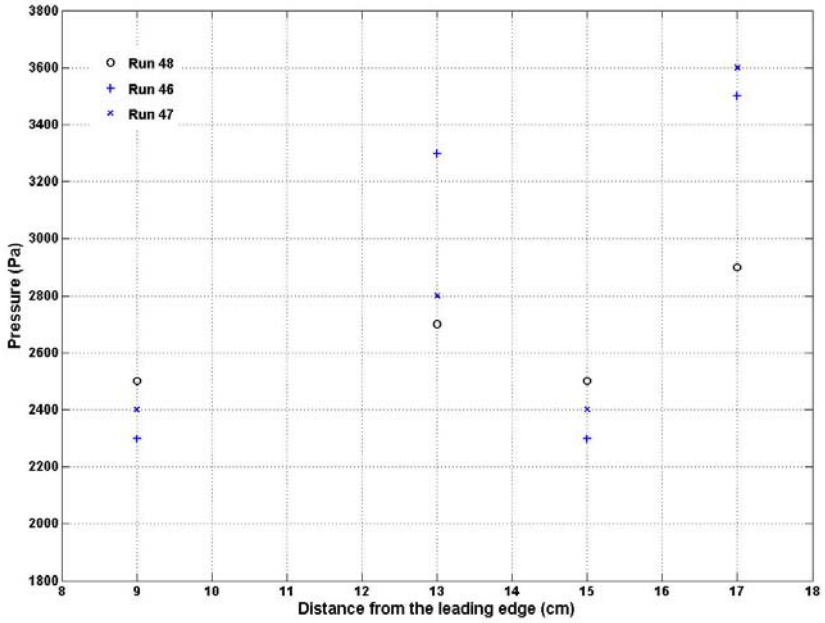

Array B

Figure.18: Effect of steady thermal bump (glow plug) with argon as test gas; Run48- without thermal bump, Run 46 and 47- with thermal bump

It can be seen from the above figures that the presence of thermal bump does alter the surface pressure distribution. At many locations there is a significant deviation from the base pressure values with the thermal bump. The effect is best seen at the last 2 sensors in Array B (near the side, 3 cm away from centerline) with argon as test gas and with a plasma pulsing frequency of 8 kHz, when the surface pressure drops there drastically to values that are lower than the measurable range of the sensors. At most of the locations there is a drop in surface pressure with the thermal bump, although there are some places where an increase is seen. There is also a significant difference observed between the cases of different actuator lengths. In terms of numbers the changes are significant.

There are a number of reasons that can be attributed to the observed changes. The investigations on the effect of DBD on low speed flows have proposed the *"Ionic wind"*, or equivalently the body force on generated charges due to the electric field, as the main factor to play with the flow field (G. I. Font et al., 2006). There are investigations that also argue in favour of the heating effects as a reason (E. Caraballo et al., 2009). There are also arguments in literature, claiming that the heat addition is of no significance in comparison with the effect of momentum addition (through ionic wind) with the DBD (U. Kogelschatz, 2003). While these arguments give an insight into the mechanisms of flow control with DBD in low speed flows, for the case of high speed flows the questions are still open. Considering the present investigations on high speed flows, the flow speed is of the order of 1000 m/s. The ionic wind (as discussed in the literature) is just of the order of 10 m/s at pressures of the order of atmospheric pressure. Considering the pressure levels of the experiments (few 1000 Pa being the freestream pressure) the ionic wind velocities are much lower, and thus are negligibly small in comparison with the freestream velocities. Thus the role of ionic wind is still a question in the present case.

It was estimated from the measured voltage and current signals that the maximum power supply was around 40 W/ cm^2 (with actuator of length 5 mm). Assuming even 10% of this supplied power gets into the flow as heat, only a few W/ cm^2 of heat would get into the flow, which is very small in comparison with the heating rates near the leading edge for the high values of enthalpy of the flow being investigated. Thus the expectation of thermal effects to have played a role in the observed changes in surface pressure, would still be an unreasonable speculation.

This would mean that the pulsing frequency of plasma could have a significant role to play. Certain modes of the flow can get excited with the pulsing. This is something that needs a closer look in the near future. But the question still remains open especially because of the observed differences in surface pressures for the cases of different plasma actuator lengths. Making the actuator smaller concentrates the discharge in smaller area, which in turn intensifies the plasma. The way by which the actuator length plays a role is the other thing to be answered.

Considering the case of steady thermal bump; here again the presence of thermal bump alters the pressure distribution, with increase at some locations and decrease at some others. This would probably be due to the localized high temperature (estimated to be 1200 K), which is comparable with the stagnation temperature of the flow itself.

Making a conclusion on the general trend and phenomenology is still a long way. Thus the present documentation is restricted to report the measured numbers as such, indicating the changes observed with the presence of the different kinds of perturbations. A closer look and a detailed investigation need to be done.

Experiments with sharp cone:

There were also parallel efforts on understanding the effect of a thermal bump on the hypersonic flow field over a sharp cone model, in IISc hypersonic shock tunnel HST2. Experiments were done by putting a steady thermal bump (a heating element) axi-symmetrically near the cone tip and the surface heat transfer rates were measured with and without the thermal bump. Further experiments towards measuring the surface heat transfer rates on the sharp cone with the pulsed thermal bump are underway and thus only a brief summary of the experiments conducted thus far with the cone model is presented subsequently.

Test model and Experimental conditions:

The test model is a 60^0 sharp cone that ends in a cylinder as shown Figure.19, which shows the schematic of the model indicating the locations of heat transfer gauges. Figure.20 shows a photograph of the model. The model has a Macor conical tip on which the heating element (a thin tungsten filament) can be placed. Figure.21 shows the model mounted within the tunnel with the heating element switched on.

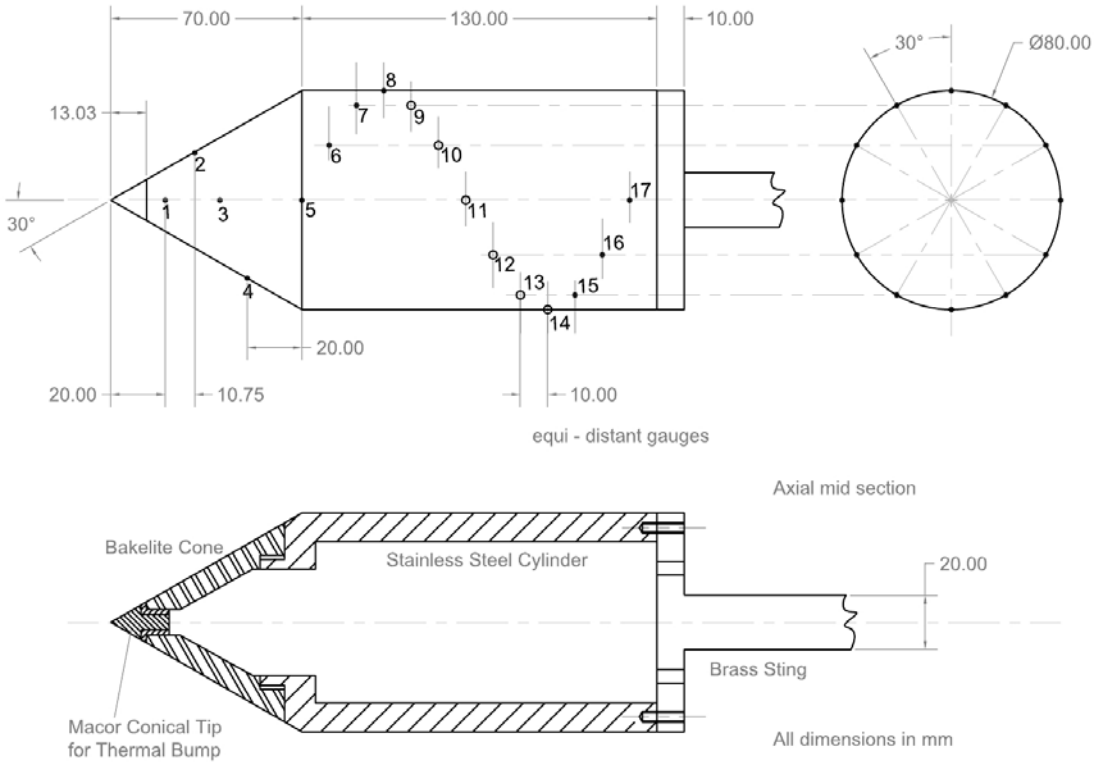

Figure.19: Schematic of the sharp cone model

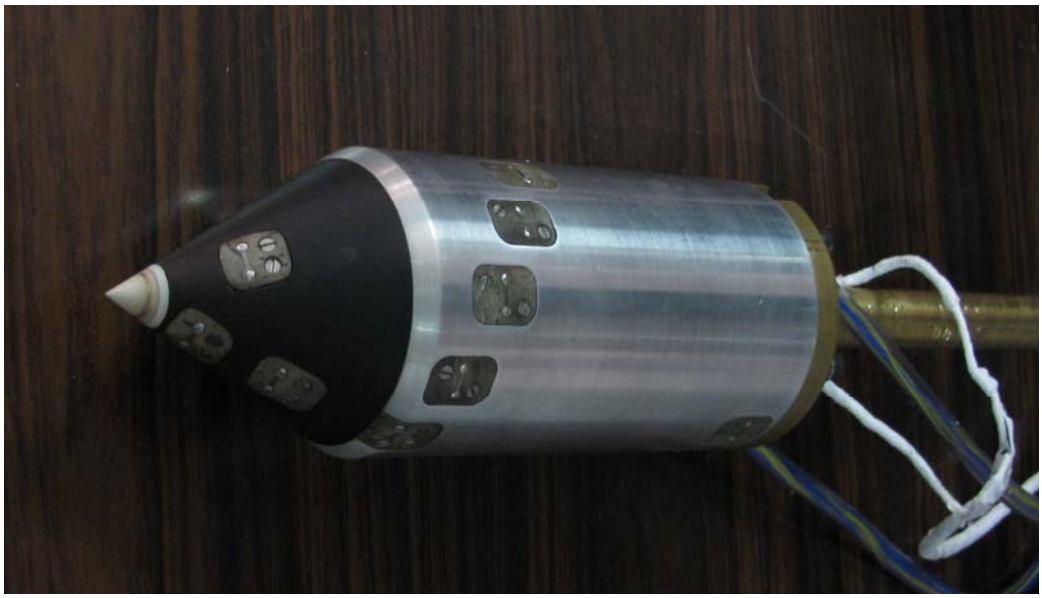

Figure.20: Photograph of the model

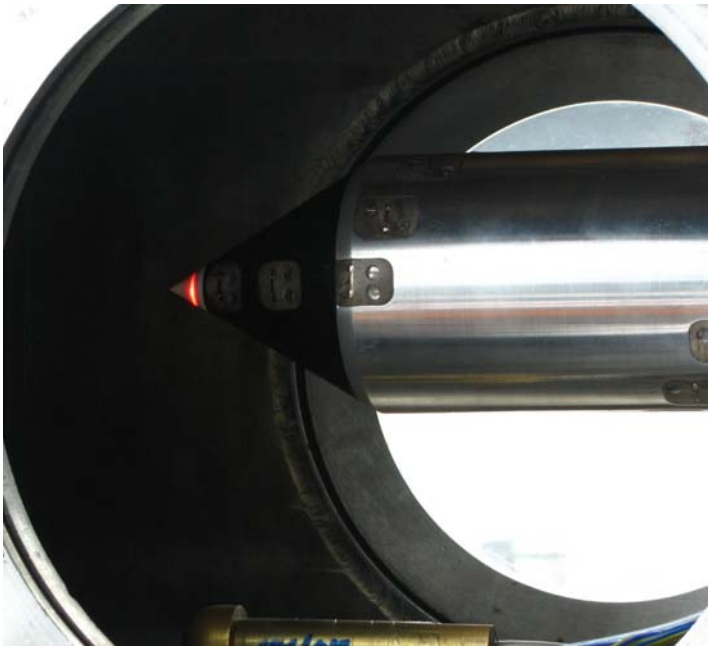

Figure.21: Photograph of the model inside the tunnel with the heating element on

The model has 17 hand painted heat transfer gauges- 4 on cone, 12 on cylinder and 1 on the junction between the cone and the cylinder. The heating element is provided with a constant current supply of 2 A and the amount of energy it adds to the flow is estimated to be roughly 9 W/ cm^2 based on the obtained voltage measurements.

Air is the test gas. The freestream conditions are estimated by means of the shock tube and pitot measurements, performed along with the experiments with the cone mode. The typical freestream conditions are the following.

Table.3: Typical freestream conditions for sharp cone experiments

M_∞	P_0 (bar)	T_0 (K)	P_∞ (Pa)	T_∞ (K)	ρ_∞ (kg/m3)	Re_∞x106 /m
8.05	**20.2**	**2026.9**	**198**	**145.2**	**0.0048**	**0.95**

Surface convective heat transfer rate measurements:

The surface heat transfer rates are measured using platinum thin film sensors sputtered on a Macor insulating substrate. Change in temperature due to flow leads to change in resistance of the thin films, which reflects on the voltage. The voltage-time signal thus obtained is indirectly the temperature time signal. Knowing the temperature coefficient of resistance and the backing material property of Macor the one-dimensional conduction equation is solved, to obtain heat transfer rate through the integration of the temperature-time signal. Figure.22 shows a comparison of the surface heat transfer rates along the model with and without thermal bump. ***Note:*** The values presented are the average of the measured heat transfer values over a number of runs (3-4 runs) per each condition. The distance from the tip is normalized by the overall length of the model.

It can be seen that close to the thermal bump the wall heat flux on the cone surface drops, but after some distance comes back to the value of the base case without thermal bump. It is at the junction between the cone and the cylinder that a drastic difference is observed. At the junction the heat flux reaches a peak without thermal bump. With thermal bump the wall heat flux at the junction is consistently found to be dropping drastically as can be seen in the figure. This interesting observation leaves an open question about the physics involved. At the cylinder portion the heat flux values are very low and thus no comment can be made of the measured values with and without thermal bump.

The Stanton number is given by,

$$St = \frac{q_w}{\{\rho_\infty u_\infty [c_p (T_o - T_w)]\}}$$

Where q_w is the wall heat flux, ρ_∞ and u_∞ are the freestream density and velocity, c_p is the specific heat of air at constant pressure, T_o is the stagnation temperature and T_w is the wall temperature. Figure.23 shows the results in terms of Stanton number against the non dimensional distance. The experimental results are plotted alongside the laminar (Hayes & Probstein, 1959) and turbulent (Stollery & Coleman, 1975) theoretical predictions.

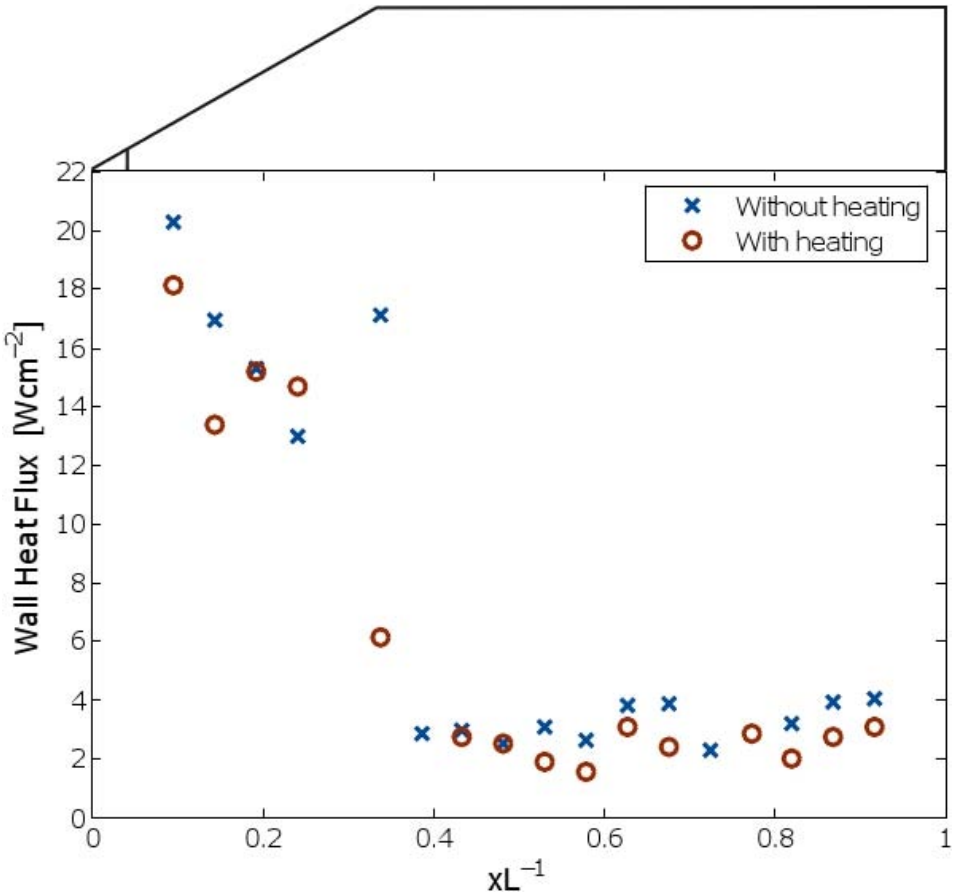

Figure.22: Wall heat flux distribution along the length of the model

Conclusions and future plan:

The presence of thermal bump (both steady and pulsating) appears to alter the pressure distribution on the flat plate at hypersonic Mach numbers. The effect of pulsating bump on the surface static pressure distribution is more pronounced compared to steady thermal bump. The decrease in the measured values of the static pressure downstream of the pulsating bump is substantial in Argon environment compared to dry air. Some of the important conclusions from the studies so far are summarized below:

- The pressure field in the presence of steady thermal bump appears to be oscillatory. At some locations downstream of the bump the static pressure decreased by ~ 25 -30% while it increased by 10-15% at other locations in the vicinity of the hot spot. However substantial reductions in the downstream pressure (30 -50%) have been measured on the flat plate in the presence of oscillating thermal bump.
- The reduction appears to be strongly dependent on the pulsing frequency. The pressure reduction seems to be better with argon as test gas compared to the experiments with dry air.

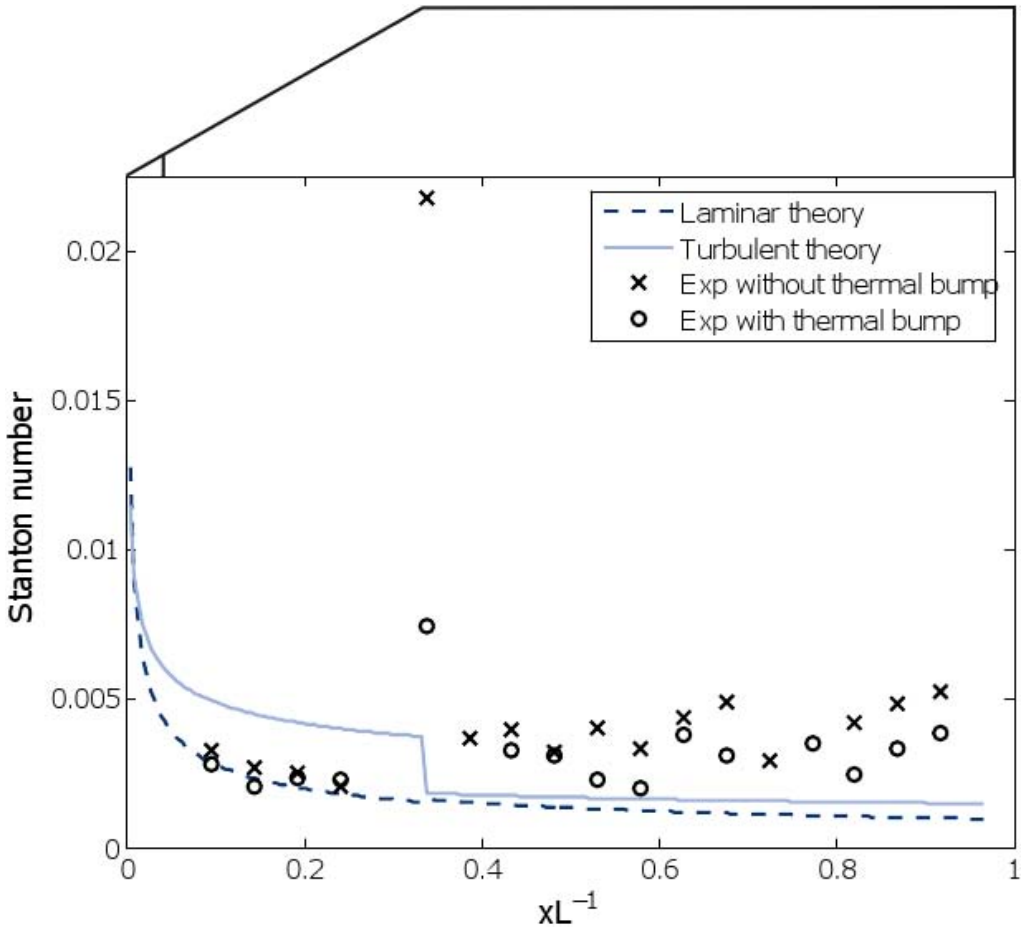

Figure.23: Stanton number variation along the cone cylinder model with and without thermal bump

- Due to the effects of electromagnetic interference and inherently lower values surface convective heat transfer rates on the flat plate in the presence of oscillatory thermal bump could not be measured.
- However, surface heat transfer rates on a cone-cylinder model in the presence of a steady thermal bump (40 W/cm^2) near the apex of the sharp cone has been measured. Drastic reduction (60%) near the cone cylinder junction has been measured in the presence of the hot spot near the cone apex at Mach 6.

A proper characterization of the plasma is underway so as to understand the parameters that can affect the flow field. A detailed analysis of the signals in the frequency domain is one of the major activities that have been planned in the next phase of the project. The additional frequencies that have been introduced into flow due to the presence of thermal bump should be found out and precise physics governing the frequency coupling between the DBD and flow frequencies needs careful examination. Because of the low operational pressure the thickness of the dielectric barrier discharge plasma is much thicker than the conventional values of DBD plasma thickness in atmospheric pressure conditions. This appears to be main reason why the oscillating thermal bump behaves like an obstruction to the flow resulting in possible flow separation downstream of the thermal bump. This also explains the low values of static pressure measured downstream of

the oscillating thermal bump. Experiments are underway to measure the surface heat transfer rates in the presence of a pulsed thermal bump (plasma), over both flat plate and cone model. The preliminary efforts showed that the heat transfer signals were largely affected by electromagnetic interference. Ways of overcoming this issue are being looked upon. The ways of improving the heat transfer measurements with the flat plate (having low values oh heating rates) are also under exploration.

References:

G. I. FONT, S. JUNG, C. L. ENLOE, T. E. McLAUGHLIN, W. L. MORGAN & J. W. BAUGHN, Simulation of the effects of force and heat production by a plasma actuator on neutral flow evolution, *44th AIAA Aerospace Science Meet & exhibit*, Reno, Nevada (2006).

E. CARABALLO, N. WEBB, J, LITTLE, J-H. KIM & M. SAMIMY, Supersonic inlet flow control using plasma actuators, *47th AIAA Aerospace Science Meet & exhibit*, Orlando, Florida (2009).

ULRICH KOGELSCHATZ, Dielectric barrier discharges: Their history, discharge physics and industrial application, *Plasma chemistry and plasma processing*, **23** (2003).

WALLACE D. HAYES & RONALD F. PROBSTEIN, Hypersonic Flow Theory, Volume 5 of Applied Mathematics and Mechanics, *Academic Press*, New York (1959).

STOLLERY J. L & COLEMAN G. T, A correlation between pressure and heat transfer distribution at supersonic and hypersonic speeds, *Aeronautical quarterly*, 304-312 (1975).

APPENDIX I

Freestream Conditions

Table.1: Freestream conditions with air as test gas

Run no	M_∞	P_0 (bar)	T_0 (K)	P_∞ (Pa)	T_∞ (K)	ρ_∞ (kg/m3)	Re_∞x106 /m
02	6.25	29.1	1474.2	1450.8	167.3	0.0302	4.30
06	6.26	29.39	1483.3	1451	167.8	0.0301	4.28
07	6.25	29.1	1474.2	1450.8	167.3	0.0302	4.30
09	6.25	29.1	1474.2	1450.8	167.3	0.0302	4.30
12	6.26	29.39	1483.3	1451	167.8	0.0301	4.28
13	6.25	29.1	1474.2	1450.8	167.3	0.0302	4.30
35	6.25	29.1	1474.2	1450.8	167.3	0.0302	4.30
36	6.26	29.39	1483.3	1451	167.8	0.0301	4.28
44	6.26	29.39	1483.3	1451	167.8	0.0301	4.28
45	6.26	29.39	1483.3	1451	167.8	0.0301	4.28
49	6.26	29.39	1483.3	1451	167.8	0.0301	4.28

Note:

Runs 01, 02 are experiments without plasma.

Runs 07 and 09 are experiments with plasma at 8000 Hz

Runs 12 and 13 are experiments with plasma at 19000 Hz

Runs 35 and 36 are experiments with plasma at 6000 Hz, with actuator of 0.5 cm.

Runs 44, 45 and 49 are experiments with glow plug mode; Runs 44 and 45 are with glow plug on and Run 49 is with glow plug off.

Table.2: Freestream conditions with argon as test gas

Run no	**M_∞**	**P_0 (bar)**	**T_0 (K)**	**P_∞ (Pa)**	**T_∞ (K)**	**ρ_∞ (kg/m3)**	**Re_∞x106 /m**
04	9.02	25.93	2208.5	633.9	78.13	0.0390	9.90
05	9.07	26.26	2228.4	625.7	78.03	0.0386	9.86
10	9.02	25.93	2208.5	633.9	78.13	0.0390	9.90
11	9.02	25.93	2208.5	633.9	78.13	0.0390	9.90
14	9.07	26.26	2228.4	625.7	78.03	0.0386	9.86
40	9.07	26.59	2248.6	633.6	78.74	0.0387	9.83
41	9.07	26.59	2248.6	633.6	78.74	0.0387	9.83
46	9.07	26.59	2248.6	633.6	78.74	0.0387	9.83
47	9.07	26.59	2248.6	633.6	78.74	0.0387	9.83
48	9.07	26.59	2248.6	633.6	78.74	0.0387	9.83

Note:

Runs 04, 05 are experiments without plasma.

Runs 10 and 11 are experiments with plasma at 8000 Hz

Run 14 is experiment with plasma at 19000 Hz

Runs 40 and 41 are experiments with plasma at 6000 Hz, with actuator of 0.5 cm.

Runs 46, 47 and 48 are experiments with glow plug mode; Runs 46 and 47 are with glow plug on and Run 48 is with glow plug off.

Measured values of surface static pressures on the flat plate model

Table.3: Surface pressures with air as test gas- Array-A

Run number	Surface pressures measured at various distances from leading edge (Pa)				
	9 mm	11 mm	13 mm	15 mm	17 mm
02	3200	3300	3800	3500	3300
06	3200	3400	3900	3500	3400
07	3400	2400	3400	2700	3000
09	3300	2400	3500	2700	3100
12	3400	3300	3800	2000	2800
13	3300	3300	3900	2200	2700
35	2900	3300	3200	1800	1700
36	3100	3300	3300	2200	1900
44	2500	2900	2700	2900	2700
45	2300	2900	2800	3000	2400
49	2500	2800	2900	3100	3100

Table.4: Surface pressures with air as test gas- Array B

Run number	Surface pressures measured at various distances from leading edge (Pa)			
	9 mm	13 mm	15 mm	17 mm
02	3800	4000	3600	4000
06	3900	4100	3500	4100
07	2000	2800	3600	3200
09	2200	2700	3400	3400
12	3600	3300	2000	4000
13	3300	3400	2100	3800
35	2900	2800	3200	4400
36	3000	2600	3200	4800
44	3000	3300	2900	3500
45	3000	3700	3100	3500
49	2800	3100	2700	3200

Table.5: Surface pressures with argon as test gas- Array-A

Run number	Surface pressures measured at various distances from leading edge (Pa)				
	9 mm	11 mm	13 mm	15 mm	17 mm
04	2800	2800	2900	2300	2500
05	2900	3000	3200	2300	2600
10	3200	2500	2500	1600	1700
11	3100	2200	2300	2000	1800

14	3000	2700	3100	Not obtained	2000
40	1500	2800	2500	1400	1600
41	2000	3100	2600	1500	1600
46	2700	2700	2400	1500	1700
47	2400	2700	2200	800	1500
48	2600	2600	2500	2700	2500

Table.6: Surface pressures with argon as test gas- Array B

Run number	**Surface pressures measured at various distances from leading edge (Pa)**			
	9 mm	**13 mm**	**15 mm**	**17 mm**
04	2500	2800	2800	2800
05	2600	2800	3000	2700
10	1800	2000	Low	Low
11	2300	2100	Low	Low
14	Not obtained	Not obtained	2500	2800
40	2500	2000	2500	4100
41	2700	2400	2600	4100
46	2300	3300	2300	3500
47	2400	2800	2400	3600
48	2500	2700	2500	2900

Appendix A

List of personal supported under this project who significantly contributed to this project:

1) Mr. Raghu Gowda Project Assistant From April 2009 – February 2010

Appendix B

Publications:

1. G. Jagadeesh, S. Sriram, S. Saravanan, K. Nagashetty and K.P.J. Reddy, "Experimental investigations on the effect of a thermal bump in the hypersonic flow around a flat plate", ***AIAA Paper 2009 -1402***, 47th AIAA Aerospace Sciences Meeting and Exhibit, Orlando, January 2009.
2. R. Sriram, Srisha Rao M.V., Raghu Narayan, G. Jagadeesh and K.P.J. Reddy, "Experimental investigations on the effects of a steady and pulsed plasma in the hypersonic flow around a flat plate", ***AIAA Paper 2010 -0262***, 48th AIAA Aerospace Sciences Meeting and Exhibit, Orlando, January 2010.